Modelling Simul. Mater. Sci. Eng. **15** (2007) S377–S392 doi:10.1088/0965-0393/15/4/S05

Micromechanical and macroscopic models of ductile fracture in particle reinforced metallic materials

Chao Hu, Jie Bai and Somnath Ghosh

Department of Mechanical Engineering, the Ohio State University, Room W496, Scott Laboratory, 201 West 19th Avenue, Columbus, OH 43210, USA

E-mail: ghosh.5@osu.edu

Received 25 November 2006, in final form 12 March 2007
Published 1 May 2007
Online at stacks.iop.org/MSMSE/15/S377

Abstract

This paper is aimed at developing two modules contributing to the overall framework of multi-scale modelling of ductile fracture of particle reinforced metallic materials. The first module is for detailed micromechanical analysis of particle fragmentation and matrix cracking of heterogeneous microstructures. The Voronoi cell FEM for particle fragmentation is extended in this paper to incorporate ductile failure through matrix cracking in the form of void growth and coalescence using a non-local Gurson–Tvergaard–Needleman (GTN) model. In the resulting enriched Voronoi cell finite element model (VCFEM) or E-VCFEM, the assumed stress-based hybrid VCFEM formulation is overlaid with narrow bands of displacement based elements to accommodate strain softening in the constitutive behaviour. The second module develops an anisotropic plasticity-damage model in the form of the GTN model for macroscopic analysis in the multi-scale material model. Parameters in this model are calibrated from results of homogenization of microstructural variables obtained by E-VCFEM analysis of microstructural representative volume element. Numerical examples conducted yield satisfactory results.

1. Introduction

Particle reinforced metallic materials, e.g. metal matrix composites, are widely used in the automotive, aerospace and other engineering systems due to their light weight and superior mechanical properties. Despite certain mechanical property enhancements, the presence of precipitates and particulates in their microstructure often affects their failure properties like fracture toughness and ductility in an adverse manner. Important micromechanical damage modes that are responsible for diminishing the overall properties include particulate fragmentation, debonding at interfaces and ductile matrix failure due to void initiation, growth and coalescence. Diminished structural integrity due to degraded failure properties has tempered the effectiveness of these materials in high performance applications. Rigorous fundamental studies reflecting the actual microstructural morphologies are required for

understanding deformation and failure mechanisms. Many particle reinforced materials exhibit strong non-uniformities in the microscale morphology and composition, e.g. in spatial distribution with regions of clustering, in reinforcement shape and size, or in different constituent material and interface properties. These morphological variations have strong effects on the microstructural damage nucleation due to particle cracking or interfacial decohesion, and matrix rupture by void growth and coalescence, culminating in crack propagation. Failure properties like strain to failure, ductility and toughness are significantly affected by these microstructural distributions.

The complex interaction between competing damage modes in the presence of non-uniform heterogeneities makes the task of failure analysis of discretely reinforced materials rather challenging. A large volume of computational studies have been conducted for understanding the elastic–plastic deformation and damage behaviour of discretely reinforced materials. Ghosal and Narasimhan [1] have studied the fracture initiation around the notch tip, while Steglich and Brocks [2] have studied the mechanism of void nucleation by interfacial debonding and particle cracking. In a comprehensive discussion on deformation and damage in particle reinforced composites, Llorca [3] has used multi-particle unit cells to investigate the influence of particle distribution on mechanical properties and ductile failure. Most of these studies focus on the initial stages of ductile damage and do not consider the effect of microstructural morphology on the evolution of ductile failure by void growth in the matrix and coalescence. There is a paucity of studies on failure modelling in the presence of reinforcements of arbitrary shapes, sizes, orientation and non-uniform spatial distribution. Ductile fracture depends on extreme values of microstructural characteristics, e.g. nearest neighbour distance, rather than the low order moments such as mean volume fraction. Hence it is particularly important to accurately represent the real microstructural characteristics in the models for predicting ductility. Ghosh *et al* have developed the Voronoi cell finite element model (VCFEM) to simulate particle cracking induced damage [4, 5] and interfacial debonding [6] in particle and fibre reinforced composites with complex non-uniform microstructural morphology. In the present work, the VCFEM is extended to incorporate ductile failure by particle fragmentation followed by matrix cracking in the form of void growth and coalescence. The non-local Gurson–Tvergaard–Needleman (GTN) model of porous plasticity [7–9] is implemented in an enriched VCFEM or E-VCFEM framework for simulating ductile fracture. In E-VCFEM, the stress-based hybrid VCFEM formulation is enriched adaptively in narrow bands of localized plastic flow and void growth, and overlaid with displacement based elements to accommodate strain softening in the constitutive behaviour.

In the second part of this paper, an anisotropic continuum damage model is developed for pressure dependent plastic materials. Such a model is necessary for macroscopic analysis in multi-scale material modelling of ductile fracture. Damage evolution is inherently a multiple-scale phenomenon where damage initiates at a microscopic scale and grows to manifest as a macroscopic crack. Effective simulators should connect events at different length scales with delineation of morphological details at each scale. It is convenient to use macroscopic constitutive laws obtained by the homogenization of variables obtained from micromechanics simulations. One of the earliest models of anisotropic ductile failure was proposed by Rice [10]. Various continuum constitutive models have been developed based on unit cell analyses of composite and porous microstructures. A number of these models are based on the GTN model. Chien *et al* [11] have investigated the influence of normal anisotropy of matrix material on the plastic behaviour of porous ductile material. Benzerga [12–14] has conducted limit analyses of representative volume element (RVE) and has incorporated microscopic plastic anisotropy and void shape effects into constitutive equation of porous ductile metal. However, most of

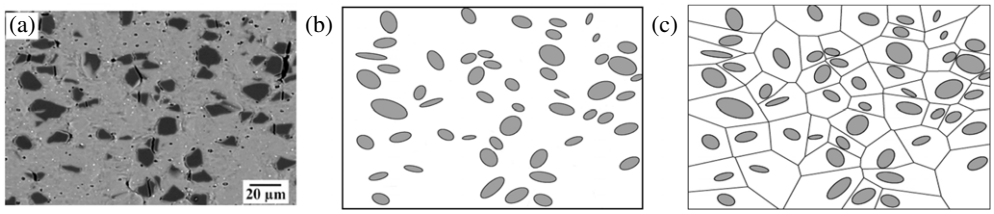

Figure 1. (*a*) An optical micrograph of a section of Al–SiC composite, (*b*) equivalent microstructure with elliptical particles, (*c*) Voronoi cell FEM mesh of the equivalent microstructure.

these models do not consider the complexity of real microstructures and damage interaction. In this paper, an anisotropic GTN type constitutive model is developed for macroscopic damage analysis in particle reinforced aluminium with non-uniform microstructure. The model is developed by homogenizing microstructural variables obtained by E-VCFEM analysis of a microstructural RVE containing particles, matrix and voids. It should be emphasized that the macroscopic model developed corresponds to a single microstructural realization and extensions to other microstructures are beyond the scope of this paper. Variations in loading, stresses, strains, etc occurring in a macroscopic structure are accommodated by the model. Extending the parameters to other microstructures with some scaling involved is a non-trivial enterprise, and will be considered in the future.

2. Enriched VCFEM for ductile fracture of particle reinforced metallic materials

As shown in figure 1, the VCFEM naturally evolves by tessellation of the microstructure into a network of multi-sided Voronoi cells. Each Voronoi cell represents the neighbourhood of heterogeneities such as particles or inclusions in the microstructure. The particles are represented as ellipses or as multi-sided polygonal domains in this paper. The particles are assumed to be brittle elastic materials while the matrix is assumed to be ductile and porous and is represented by a pressure dependent elasto-plastic material model.

The VCFEM [4–6] formulation is based on the assumed stress hybrid formulation, in which equilibrated stress fields are assumed in the interior of each element and compatible displacements are assumed on the boundary of each element and on the particle–matrix interface. After particle cracking, the topology of each element changes from two constituent phases to three constituents with the inclusion of the crack, as shown in figure 2. In the subsequent ductile fracture phase, regions in each Voronoi cell that exhibit softening in the stress–strain behaviour are enriched adaptively with finite deformation, displacement based finite elements. The enriched Voronoi cell consists of the matrix phase Ω_m, the particle phase Ω_c and a softening region of ductile damage Ω_s, as shown in figure 3.

With continuing deformation beyond the stage of cracked particles, material points in the matrix lose their load carrying capacity due to local void growth and strain softening. These regions are identified and adaptively converted to softened regions Ω_s. A displacement based finite element mesh is automatically generated in narrow localized regions of strain softening. Stresses σ_{ij}^s in these regions are generated by using finite deformation kinematics with an implicit backward Euler integration rule [15]. For the superposed displacement elements, a type of h-type of refinement strategy proposed in [16] is used to reduce discretization error in the local solution. The B-bar method in [17] is used for avoiding dilatational locking with nearly incompressible plasticity. The rotated Cauchy stress rate [18,22] is used as an objective

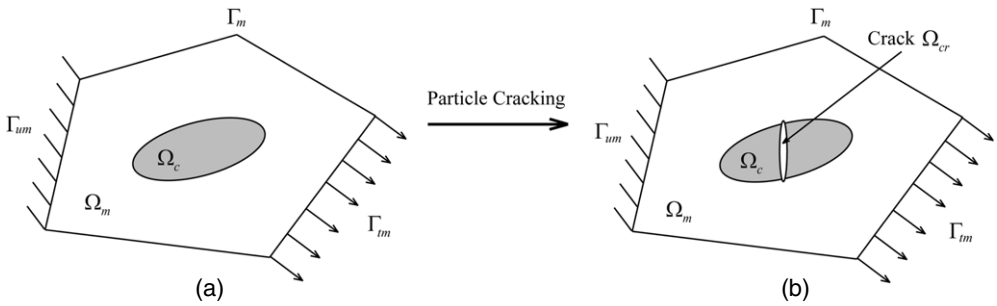

Figure 2. Evolution of a Voronoi cell element (*a*) without damage and (*b*) with particle cracking.

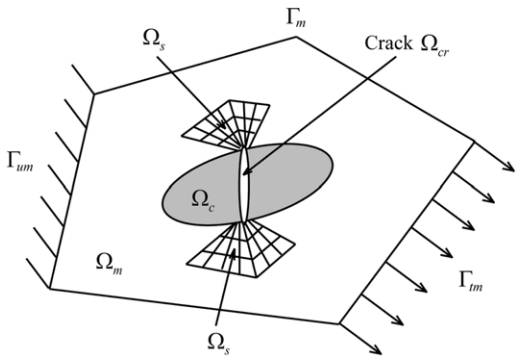

Figure 3. Enriched VCFEM with superposed finite deformation displacement elements in regions of high local void volume fraction Ω_s

stress measure for the finite deformation formulation. The entire description of E-VCFEM is quite long and is beyond the scope of this paper. A summary is presented here, but details are being prepared for a future paper [29].

2.1. VCFEM formulation with particle cracking

For particle cracking in an elastic–plastic matrix, an incremental element energy functional Π_e^{PC} is defined for each Voronoi cell element in terms of stress increments in the matrix and particle phases $\Omega_m \cup \Omega_c$, and displacement increments on the element boundary $\partial\Omega_e$, particle–matrix interface $\partial\Omega_c$ as well as on the crack boundary $\partial\Omega_{\mathrm{cr}}$. The first variation of Π_e^{PC} is expressed as

$$\begin{aligned}\delta\Pi^{\mathrm{PC}}{}_e(\Delta\sigma_{ij}, \Delta\bar{u}_i) = &-\int_{\Omega_m\cup\Omega_c} \Delta\varepsilon_{ij}\delta\Delta\sigma_{ij}\mathrm{d}\Omega - \int_{\Omega_m\cup\Omega_c} \varepsilon_{ij}\delta\Delta\sigma_{ij}\mathrm{d}\Omega \\ &+ \int_{\partial\Omega_e} \delta\Delta\sigma_{ij}n_j^e\Delta\bar{u}_i\mathrm{d}\partial\Omega + \int_{\partial\Omega_e} (\sigma_{ij}+\Delta\sigma_{ij})n_j^e\delta\Delta\bar{u}_i\mathrm{d}\partial\Omega \\ &- \int_{\Gamma_{tm}} (\bar{t}_i+\Delta\bar{t}_i)\delta\Delta u_i\mathrm{d}\Gamma - \int_{\partial\Omega_c} (\delta\Delta\sigma_{ij}^m - \delta\Delta\sigma_{ij}^c)n_j^c\Delta\bar{u'}_i\mathrm{d}\partial\Omega \\ &- \int_{\partial\Omega_c} (\sigma_{ij}^m+\Delta\sigma_{ij}^m-\sigma_{ij}^c-\Delta\sigma_{ij}^c)n_j^c\delta\Delta\bar{u'}_i\mathrm{d}\partial\Omega \\ &- \int_{\partial\Omega_{\mathrm{cr}}} \delta\Delta\sigma_{ij}^c n_j^{\mathrm{cr}}\Delta\bar{u''}_i\mathrm{d}\partial\Omega - \int_{\partial\Omega_{cr}} (\sigma_{ij}^c+\Delta\sigma_{ij}^c)n_j^{\mathrm{cr}}\delta\Delta\bar{u''}_i\mathrm{d}\partial\Omega. \end{aligned} \tag{1}$$

Here $\bar{\boldsymbol{t}}$ is the external traction on the traction boundary Γ_{tm} and n is the outward normal on respective boundary segments. The corresponding total energy functional for the entire computational domain is expressed as $\sum_{e=1}^{\mathrm{NEL}} \Pi_e^{\mathrm{PC}}$. The following Euler's equations are obtained from the stationarity conditions of the functional:

$$\begin{aligned}
&\nabla\Delta\boldsymbol{u} = \Delta\varepsilon \text{ in } \Omega_e; \qquad (\boldsymbol{\sigma} + \Delta\boldsymbol{\sigma}) \cdot \boldsymbol{n}^{e+} = -(\boldsymbol{\sigma} + \Delta\boldsymbol{\sigma}) \cdot \boldsymbol{n}^{e-} \text{ on } \partial\Omega_e; \\
&\qquad (\boldsymbol{\sigma} + \Delta\boldsymbol{\sigma}) \cdot \boldsymbol{n}^{e+} = \bar{\boldsymbol{t}} + \Delta\bar{\boldsymbol{t}} \text{ on } \Gamma_{tm} (\boldsymbol{\sigma}^c + \Delta\boldsymbol{\sigma}^c) \cdot \boldsymbol{n}^c \\
&\qquad = (\boldsymbol{\sigma}^m + \Delta\boldsymbol{\sigma}^m) \cdot \boldsymbol{n}^c \text{ on } \partial\Omega_c; (\boldsymbol{\sigma}^c + \Delta\boldsymbol{\sigma}^c) \cdot \boldsymbol{n}^{\mathrm{cr}} = \boldsymbol{0} \text{ on } \partial\Omega_{\mathrm{cr}}.
\end{aligned} \tag{2}$$

Superscript + and − correspond to elements on both sides of the boundary $\partial\Omega_e$. The equilibrated stress field σ_{ij} is interpolated independently in the matrix and particle phases of each Voronoi cell element. Conveniently, the Airy's stress function $\tilde{\Phi}(x, y)$ is used to derive the equilibrated stress increments in the VCFEM formulation for rate independent elasto-plasticity [4–6]. Compatible displacement fields $\Delta\bar{u}_i$ are independently interpolated on the element/particle/crack boundaries using standard shape functions for line elements. *A priori* assumptions on equilibrated stress increments $\Delta\sigma_{ij}$ and constitutive relationships along with Euler equations completely define the boundary value problem for a heterogeneous domain undergoing particle cracking.

The VCFEM has been successfully applied for the simulation of particle cracking in reinforced metal matrix composites [4,5]. Complete particle cracking is assumed to occur at the onset of damage, thereby avoiding crack propagation within each particle. A high aspect ratio ellipse ($a/b = 10$) is used to represent the crack in the particle [4,19]. The particle crack initiation criterion is expressed in the form of a Weibull probability function that depends on the local principal stresses and the volume of the particles in the composite [5,19]. For the ith particle, the probability of fracture P_i is expressed as

$$P_i(v, \sigma_i^{\mathrm{I}}) = 1 - \exp\left[-\frac{v}{v_0}\left(\frac{\sigma_i^{\mathrm{I}}}{\sigma_{\mathrm{w}}}\right)^m\right], \tag{3}$$

where m and σ_{w} are the Weibull modulus and the characteristic strength, respectively, v is the volume of the ith particle, v_0 is a reference volume taken as the average volume of all particles and σ_i^{I} is the maximum principal stress in the ith particle.

2.2. VCFEM formulation with particle and matrix cracking causing ductile fracture

Ductile failure occurs by the combined phenomena of crack nucleation, micro-void growth and eventual void coalescence. Voids nucleate by particle fragmentation, subsequently grow in the matrix with large plastic deformation, and finally coalesce with each other to advance the local fracture zone. A non-local form of the GTN model proposed in [7,8] is used to model the post-nucleation ductile fracture in the matrix material. In this model, a pressure dependent yield surface Φ is written in terms of the evolving void volume fraction f^* as

$$\Phi = \left(\frac{q}{\sigma_0}\right)^2 + 2f^* q_1 \cosh\left(-\frac{3q_2 p}{2\sigma_0}\right) - (1 + q_3 f^{*2}), \tag{4}$$

where q and p are, respectively, the equivalent Von–Mises stress and hydrostatic pressure in the matrix, and q_1, q_2, q_3 are constants calibrated from numerical analyses of a periodic array of voids. $\sigma_0(\varepsilon^p)$ is the strength of the matrix material in the absence of voids. To avoid inherent mesh sensitivity of numerical failure predictions, a non-local evolution equation for the void volume fraction [7–9] is implemented. The non-local void volume fraction growth rate at a

material point $\boldsymbol{x}$ is written as

$$\dot{f}_{nl} = \frac{1}{W(\boldsymbol{x})} \int_{\Omega_m} \dot{f}(\bar{\boldsymbol{x}}) w(|\boldsymbol{x} - \bar{\boldsymbol{x}}|)\, \mathrm{d}\Omega; \qquad W(\boldsymbol{x}) = \int_{\Omega_m} w(|\boldsymbol{x} - \bar{\boldsymbol{x}}|)\, \mathrm{d}\Omega, \tag{5}$$

$$w(z) = \left[\frac{1}{1 + (z/L)^p}\right]^q, \qquad p = 8,\ q = 2.$$

The weighting function $w(z) = 1$ at $z = 0$, $w(z) = 0.25$ at $z = L$ a characteristic length scale and vanishes rapidly outside of the radius L. The explicit introduction of the length scale L regularizes the localization problem and prevents the matrix crack from being unreasonably small. In the E-VCFEM, L is chosen as a fraction of the maximum size of the Voronoi cell finite elements. The characteristic length L has been reported to correspond to the nearest neighbour distance between particles. The size of the Voronoi cell is representative of the nearest neighbour distance between particles. Consequently, a length scale corresponding to representative size of Voronoi cell elements is meaningful. The local void growth rate is governed by the relation:

$$\dot{f} = (1 - f_{nl})\ \dot{e}^p_{kk} + A(\bar{\varepsilon}^p)\dot{\bar{\varepsilon}}^p, \tag{6}$$

where the evolution of effective plastic strain is written as

$$\sigma_0 \dot{\bar{\varepsilon}}^p = \sigma_{ij} \dot{\lambda} \frac{\partial \Phi}{\partial \sigma_{ij}}. \tag{7}$$

The second term in equation (6) is for void nucleation controlled by plastic strain as suggested in [20], where

$$A = \frac{f_{\mathrm{N}}}{s_{\mathrm{N}}\sqrt{2\pi}} \exp\left[-\frac{1}{2}\left(\frac{\bar{\varepsilon}^p - \varepsilon_{\mathrm{N}}}{s_{\mathrm{N}}}\right)^2\right]. \tag{8}$$

For the void coalescence, an acceleration function proposed in [21] is used,

$$f^* = \begin{cases} f_{nl} & f_{nl} \leqslant f_c, \\ f_c + \frac{f^*_u - f_c}{f_f - f_c}(f_{nl} - f_c) & f_{nl} > f_c. \end{cases} \tag{9}$$

Here f_c is the critical void volume fraction at which void coalescence first occurs and f_f is the value at final failure which means the material loses all load carrying capacity as $f_{nl} \to f_f (f^* \to f^*_u = 1/q_1)$. To avoid the numerical difficulties, $(f_{nl} \to 0.95 f_f)$ is used instead of $(f_{nl} \to f_f)$ as suggested in [1].

A problem that arises with the stress-based VCFEM formulation arises from the fact that at the transition from the hardening to the softening portion of the stress–strain response, numerical instabilities result from the non-uniqueness in displacement behaviour. To avert this shortcoming, the softening region Ω_s within each Voronoi cell element is adaptively augmented with a patch of displacement based finite elements as shown in figure 3. Finite deformation, pressure dependent elasto-plasticity formulation is used for the displacement finite elements in the local softening region.

Once the patches of displacement based local elements are overlaid in the region Ω^s in each Voronoi cell element, a parameter mapping process maps the local stresses, strains and material internal variables from element domain in VCFEM to the displacement elements. A superscript s corresponds to variables associated with the enriched softening regions Ω^s. The formulation guarantees that the displacement field $\boldsymbol{u}^s$ on the boundary $\partial\Omega_s$ is compatible with the displacement fields $\bar{\boldsymbol{u}}$, $\bar{\boldsymbol{u}}'$ and $\bar{\boldsymbol{u}}$" on $\partial\Omega_m$, $\partial\Omega_c$ and $\partial\Omega_{\mathrm{cr}}$, respectively, i.e.

$$\boldsymbol{u}^s = \bar{\boldsymbol{u}} \text{ on } \partial\Omega_s \cap \partial\Omega_m; \qquad \boldsymbol{u}^s = \bar{\boldsymbol{u}'} \text{ on } \partial\Omega_s \cap \partial\Omega_c; \qquad \boldsymbol{u}^s = \bar{\boldsymbol{u}''} \text{ on } \partial\Omega_s \cap \partial\Omega_{\mathrm{cr}}. \tag{10}$$

With the addition of enriched elements in the softening region Ω_s, the VCFEM formulation is modified with an augmentation of the energy functional in equation (1). The corresponding incremental potential energy for the displacement elements with appropriate boundary conditions are added to the incremental element energy functional Π_e^{PC} to yield an enriched energy functional Π_e^{EN} with an additional independent variable $\Delta \boldsymbol{u}^s$. The first variation of Π_e^{EN} is written as

$$\delta \Pi^{\mathrm{EN}}{}_e(\Delta\sigma_{ij}, \Delta\bar{u}_i, \Delta u_i^s) = \delta\Pi_e^{\mathrm{PC}} - \int_{\Omega_s} (\sigma_{ij}^s + \Delta\sigma_{ij}^s)\delta\Delta\varepsilon_{ij}^s \mathrm{d}\Omega + \int_{\partial\Omega_s} \delta\Delta\sigma_{ij} n_j^s \Delta u_i^s \mathrm{d}\partial\Omega$$
$$+ \int_{\partial\Omega_s} (\sigma_{ij} + \Delta\sigma_{ij}) n_j^s \delta\Delta u_i^s \mathrm{d}\partial\Omega, \tag{11}$$

where Δu_i^s is the displacement increment for displacement elements. The displacement interpolation in terms of the nodal displacements are expressed as

$$\{\Delta \boldsymbol{u}^s\} = \{\boldsymbol{N}^s\}\{\Delta \boldsymbol{q}^s\}. \tag{12}$$

Additional Euler equations resulting from equation (10) are:

$$(\boldsymbol{\sigma} + \Delta\boldsymbol{\sigma}) \cdot \boldsymbol{n}^s = (\boldsymbol{\sigma}^s + \Delta\boldsymbol{\sigma}^s) \cdot \boldsymbol{n}^s \quad \text{on } \partial\Omega_s; \qquad \Delta \boldsymbol{u}^s = \Delta\bar{\boldsymbol{u}} \quad \text{on } \partial\Omega_s \cap \partial\Omega_m$$
$$\Delta \boldsymbol{u}^s = \Delta\bar{\boldsymbol{u}}' \quad \text{on } \partial\Omega_s \cap \partial\Omega_c; \qquad \Delta \boldsymbol{u}^s = \Delta\bar{\boldsymbol{u}}'' \quad \text{on } \partial\Omega_s \cap \partial\Omega_{\mathrm{cr}} \tag{13}$$

The first Euler equation in (13) ensures the traction reciprocity at the interface $\partial\Omega_s$ of the enriched region within the regular Voronoi cell element domain. The next three equations ensure the displacement increment continuity at the interfaces $\partial\Omega_s \cap \partial\Omega_m$, $\partial\Omega_s \cap \partial\Omega_c$ and $\partial\Omega_s \cap \partial\Omega_{\mathrm{cr}}$.

2.2.1. Integration algorithms in the E-VCFEM formulation. The adapted E-VCFEM couples a small deformation hybrid stress-based finite element formulation in the region Ω_m with a finite deformation displacement based finite element formulation in the softening region Ω_s. This necessitates different time-integration or stress–strain update algorithms for different regions of the element. In the stress-based hybrid region a strain update algorithm implementing the *Regula Falsi* scheme is used to calculate plastic strains, stresses and state variables for a given stress increment $\Delta\boldsymbol{\sigma}$ as discussed in [4, 5]. For the displacement elements, a backward Euler method proposed in [15] is used for stress and plastic strain update in an updated Lagrangian formulation, as introduced in [22]. The formulation uses an objective rate of the rotated Cauchy stress $\boldsymbol{\sigma}_{\boldsymbol{R}}^s = \boldsymbol{R}^{\mathbf{T}}\boldsymbol{\sigma}^s\boldsymbol{R}$, in which $\boldsymbol{R}$ is a proper orthogonal tensor representing pure rotation obtained from the polar decomposition of $\boldsymbol{F}$, i.e. $\boldsymbol{R} = \boldsymbol{F}\boldsymbol{U}^{-1}$ decomposition. The subscript 'R' corresponds to variables in a rotated configuration. The rotated Cauchy stress is updated to the $(n+1)$th increment using the equation

$$(\boldsymbol{\sigma}_{\boldsymbol{R}}^s)^{n+1} = (\boldsymbol{\sigma}_{\boldsymbol{R}}^s)^n + \Delta\boldsymbol{\sigma}_{\boldsymbol{R}}^s; \qquad \text{where } \Delta\boldsymbol{\sigma}_{\boldsymbol{R}}^s = (\boldsymbol{C}^{\mathbf{e-p}})^{n+1} : \boldsymbol{\Delta}\boldsymbol{\varepsilon}_{\boldsymbol{R}}^s \tag{14}$$

and $\boldsymbol{C}^{\mathbf{e-p}}$ is the elastic–plastic tangent stiffness in the rotated configuration, given as

$$C_{ijkl}^{\mathrm{e-p}} = \left(\frac{\partial(\boldsymbol{\sigma}_{\boldsymbol{R}}^s)_{ij}}{\partial(\boldsymbol{\varepsilon}_{\boldsymbol{R}}^s)_{kl}}\right). \tag{15}$$

An iterative solution procedure is used in the backward Euler integration method.

2.2.2. Mapping state variable from assumed stress to assumed displacement regions in VCFEM. Once the displacement elements are identified and superposed in the localized regions of high void volume fraction in E-VCFEM, it is important to map all the parameters, e.g. stress, strain and other internal variables from the assumed stress model with stress

interpolations to the assumed displacement elements. The super-convergent patch recovery or SPR method in [23] is used to map variables from the VCFE mesh to nine-noded isoparametric Lagrangian elements. In this process, a complete 4th order polynomial expansion is used for all parameters to be mapped, i.e.

$$v_p^* = \boldsymbol{P}\boldsymbol{a}, \qquad \boldsymbol{P} = [1, x, y, x^2, xy, y^2, x^3, x^2y, xy^2, y^3, x^4, x^3y, x^2y^2, xy^3, y^4], \tag{16}$$

where v_p^* represents components of stress, strain, equivalent plastic strain $\bar{\varepsilon}^p$ and void volume fraction f at nodal points of the displacement elements and $\boldsymbol{a}$ is a set of unknown coefficients. The corresponding parameters at integration points are interpolated from nodal values using shape functions for nine-noded elements

$$v = \boldsymbol{N}\boldsymbol{v}_p^*. \tag{17}$$

2.3. A numerical example of ductile failure in a reinforced aluminium microstructure

Figure 1(*a*) shows the micrograph of a reinforced Al–SiC composite consisting of 52 SiC particles. Figure 1(*c*) shows the corresponding Voronoi cell mesh for an equivalent simulated microstructure. The Al matrix is assumed to be ductile and is modelled by elastic–plasticity constitutive relations for porous materials with the following properties: Young's modulus $E = 66$ GPa, Poisson's ratio $v = 0.33$ and initial void volume fraction $f_0 = 0.004$. The post-yield behaviour for the pure matrix material without voids is expressed by the Ramberg–Osgood law ($\sigma_m = \sigma_0(\varepsilon_m^p/\alpha\varepsilon_0)^{1/n}$), where the initial flow stress of the matrix $\sigma_0 = 440$ MPa, ε_0 is the strain at yield ($\varepsilon_0 = \sigma_0/E$), $\alpha = 3/7$ and the strain hardening exponent $n = 12.5$. Certain aluminium alloys, especially rolled products with elongated grains, show anisotropy, as considered in [13]. However, many alloys also have equiaxed grains without significant anisotropy, and hence isotropic constitutive laws are considered for the aluminium matrix in this paper. The reinforcing SiC particles are assumed to be brittle and are modelled with the linear elastic properties: Young's modulus $E = 400$ GPa and Poisson's ratio $v = 0.2$. For particle cracking, $m = 2.4$, $\sigma_w = 1.32$ GPa are used in equation (3) for the Weibull model. For the GTN model, $q_1 = 1.5$, $q_2 = 1.0$, $q_3 = q_1^2 = 2.25$ are used in equation (4) and a characteristic length scale $L = 0.05 \times$ (maximum size of the Voronoi cell elements) is used in equation (5) for the non-local model. The nucleation parameters ($\varepsilon_N = 0.1$, $s_N = 0.1$, $f_N = 0.08$) are used in equation (8). The microstructure is subjected to a macroscopic tensile strain $\bar{\varepsilon}_{xx} = 1.0\%$, applied on the left side of the domain. Results of the simulation are shown in figure 4. Figure 4(*a*) shows the macroscopic strain-stress response, with the explicit effect of particle cracking followed by ductile matrix fracture. The cracked particle numbers are shown in figure 4(*b*). The first nine particles crack in isolation and do not show any softening in the stress–strain behaviour. Softening, manifested by a drop in the stress–strain curve, starts after the tenth particle has cracked followed by significant plastic deformation and void growth in the matrix. From figure 4(*b*), it is evident that the subsequent sequence of particle and matrix cracking occur in a very narrow band of the microstructure and hence a dominant crack path is observed. The sequence of particle cracking is shown in the stress–strain plot of figure 4(*a*). Contour plots of the void volume fraction in the matrix (with $f_c = 0.15$, $f_f = 0.25$), the equivalent plastic strain and the stress in the loading direction for $\bar{\varepsilon}_{xx} = 0.89\%$ are shown in figures 4(*b*)–(*d*). Near the dominant fracture path, the stress σ_{xx} decreases to near zero.

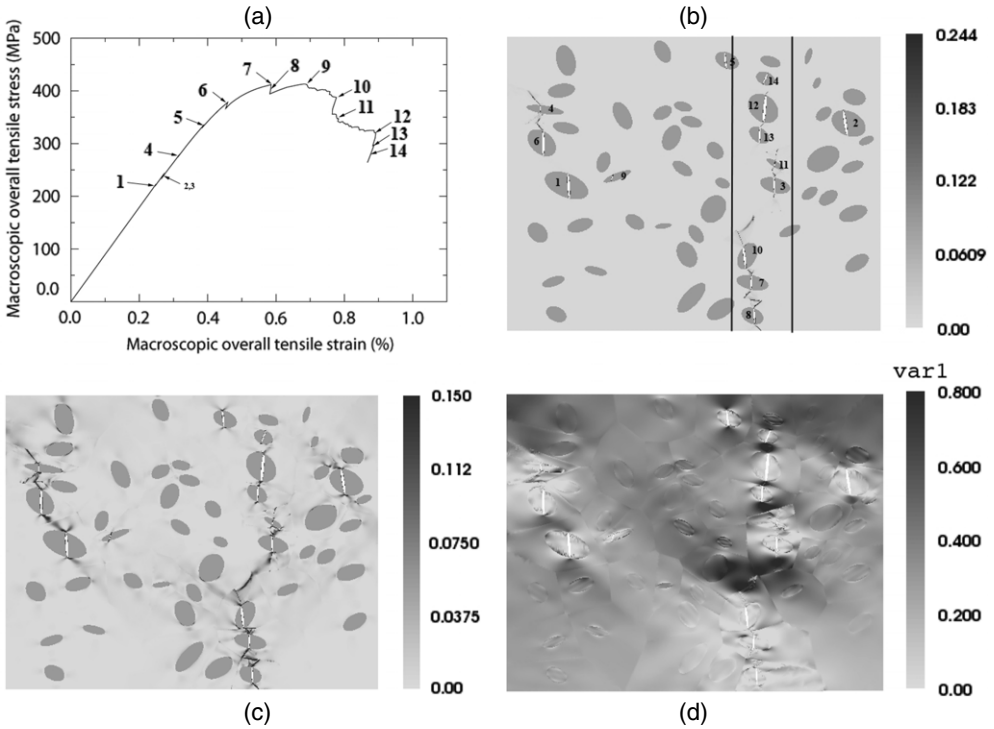

Figure 4. (*a*) Macroscopic strain–stress response; contour plots of (*b*) the void volume fraction, (*c*) the equivalent plastic strain and (*d*) the stress σ_{xx} (GPa) at $\bar{\varepsilon}_{xx} = 0.84\%$. The numbers in figures (*a*), (*b*) indicate the sequence of particle cracking.

3. Anisotropic continuum damage model for ductile materials from micromechanical analysis with homogenization

A macroscopic anisotropic damage model for plane strain analysis of ductile failure of non-uniform composites is developed in this section. The anisotropic damage model in this development has been chosen to follow the GTN model framework, but is expressed in the principal material and principal damage coordinate systems. A pre-matrix cracking version of the model, microscopic particle cracking only, has been developed by Ghosh in [24].

3.1. A macroscopic anisotropic GTN model

The macroscopic anisotropic GTN model for materials undergoing microstructural ductile fracture presented in this section only considers the growth in void volume fraction f for the plane strain problem. Void nucleation and coalescence are in the process of being incorporated in the model and will be reported in future papers. An anisotropic, hydrostatic stress and porosity dependent yield criterion is written in terms as

$$\Phi^{\text{an}} = \frac{\Sigma_{\text{eq}}^2}{Y_f^2(W_p)} + 2Q_1 f \cosh\left(\frac{Q_a\Sigma_{xx} + Q_b\Sigma_{yy} + Q_c\Sigma_{zz}}{Y_f(W_p)}\right) - 1 - (Q_1 f)^2 = 0, \tag{18}$$

where Σ_{ij} is the macroscopic stress, W_p is the plastic work and Y_f is the flow stress in shear. As stated in equation (6), the evolution of f is governed by the plastic strain and its rate, as

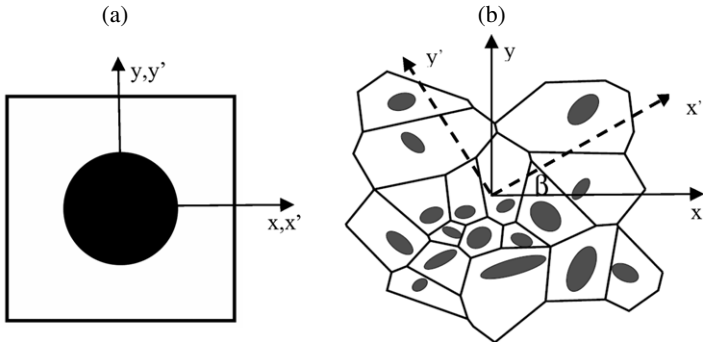

Figure 5. RVEs showing principal axes of material anisotropy (x', y'): (*a*) RVE with one circular particle, (*b*) RVE with 17 randomly distributed elliptical particles.

well as f itself. The increment of macroscopic plastic strain is then obtained from the yield criterion by using an associated flow rule for hardening materials, i.e. $\dot{e}^p_{ij} = \dot{\lambda}(\partial\Phi/\partial\Sigma_{ij})$.

For plane strain, the equivalent macroscopic stress Σ_{eq} in the material without voids (microstructure consisting of matrix and particles) is represented using Hill's [28] anisotropic yield function as

$$\Sigma^2_{\text{eq}} = F(W_p)(\Sigma_{yy} - \Sigma_{zz})^2 + G(W_p)(\Sigma_{zz} - \Sigma_{xx})^2 + H(W_p)(\Sigma_{xx} - \Sigma_{yy})^2 + C(W_p)\Sigma^2_{xy}. \tag{19}$$

The anisotropy parameters $F(W_p)$, $G(W_p)$, $H(W_p)$ and $\mathrm{C}(W_p)$ are functions of the plastic work W_p that are calibrated from homogenization studies with materials without voids. Likewise, the hydrostatic stress parameters $Q_1(W_p)$, $Q_a(W_p)$, $Q_b(W_p)$ and $Q_c(W_p)$ are calibrated from homogenization studies with voided materials. The homogenization of microscopic variables in the microstructural RVEs uses asymptotic expansion of the field variables and periodicity assumptions on the boundary, as discussed [24,27]. Homogenization studies in this work are conducted with the micromechanical E-VCFEM analysis. Methods of determination of microstructural RVEs have been discussed in detail in [25,26]. All these calibrated parameters are expected to vary with different RVEs and their calibration process is discussed in section 3.2. When $f = 0$, equation (17) reduces to the yield criterion for an anisotropic non-porous composite material as

$$\frac{F(W_p)(\Sigma_{yy} - \Sigma_{zz})^2 + G(W_p)(\Sigma_{zz} - \Sigma_{xx})^2 + H(W_p)(\Sigma_{xx} - \Sigma_{yy})^2 + C(W_p)\Sigma^2_{xy}}{Y^2_f(W_p)} - 1 = 0. \tag{20}$$

This yield criterion is defined in the principal axes of material anisotropy. Axes of material anisotropy are determined by the morphology of microstructures, such as size, shape and distribution of particles. The angle β in figure 5(*b*) corresponds to the principal axes of anisotropy and is determined from the equation:

$$\beta = \frac{1}{2}\tan^{-1}\left(\frac{2I_{xy}}{I_{xx} - I_{yy}}\right), \tag{21}$$

where $I_{xx}(= \int_A y^2 \mathrm{d}A)$, $I_{yy}(= \int_A x^2 \mathrm{d}A)$ and $I_{xy}(= \int_A xy \mathrm{d}A)$ are 2nd moments of inertia of the RVE. The moments are evaluated by pixel-based numerical integration over the area covered by all particles.

3.2. Evaluation of constitutive parameters in the macroscopic model

3.2.1. $Y_f(W_p)$ and C in equation (20). Since $Y_f(W_p)$ is the flow stress in shear, the parameter C is set to be 3. A macro–micro boundary value problem is solved with RVE homogenization, under incremented simple shear loading. This is done by applying pure macroscopic shear strain on the RVE with periodic boundary conditions, as detailed in [24]. The macroscopic plastic work is evaluated by averaging the micromechanical plastic work, i.e. $\dot{W}_p = \frac{1}{\Omega}\int_\Omega \sigma_{ij}\dot{\varepsilon}^p_{ij}\mathrm{d}\Omega$, and then the flow stress is evaluated as $Y_f(W_p) = \sqrt{3}\Sigma_{xy}$, which is then plotted as a function of W_p.

3.2.2. Parameters F, G and H.

(i) A set of numerical experiments for the RVE, without voids or particle fragmentation, are conducted using E-VCFEM for different loading conditions, represented by various macroscopic strain combinations, $e_{xx} : e_{yy} = 1 : a$, where $a = 0, 0.1, 0.2, 0.3, 0.4, 0.5, 0.6, 0.7, 0.8, 0.9$ and 1.0, respectively, corresponding to a total of 11 numerical experiments. Using homogenization theory, the macroscopic stress and strain for each case are obtained from the relations:

$$\Sigma_{ij} = \frac{1}{\Omega}\int_\Omega \sigma_{ij}(\Omega)\mathrm{d}\Omega, \qquad e_{ij} = \frac{1}{\Omega}\int_\Omega \varepsilon_{ij}(\Omega)\,\mathrm{d}\Omega. \tag{22}$$

The macroscopic stresses are plotted as functions of W_p.

(ii) Assuming that the plastic work W_p is invariant with respect to the loading condition, macroscopic stress components are obtained as functions of W_p for different loading conditions from the stress- W_p plots of step (i). Anisotropic parameters F, G and H are then evaluated by using the least squares method with equation (20) for given macroscopic plastic work W_p. This step is repeated for different values of W_p and the anisotropic parameters are plotted as functions of W_p.

3.2.3. Parameters Q_1, Q_a, Q_b and Q_c.

(i) The same set of numerical experiments for the RVE is again performed for the material with evolving void volume fraction f. The macroscopic stresses and averaged f are plotted as functions of W_p, where the averaged incremental plastic work

$$\dot{W}_p = \frac{1}{\Omega}\int_\Omega \frac{1}{1-f}\sigma_{ij}\dot{\varepsilon}^p_{ij}\,\mathrm{d}\Omega.$$

(ii) Again, assuming that W_p is invariant with respect to the load condition, the parameters Q_1, Q_a, Q_b and Q_c are evaluated by using the least squares method with equation (17). This step is repeated for different values of W_p, and Q_1, Q_a, Q_b and Q_c are plotted as functions of W_p.

The calibrated parameters which do not correspond to particle fragmentation will be considered in a future paper.

3.3. Numerical implementation

The macroscopic constitutive laws for the ductile matrix composite material undergoing ductile damage is derived from the anisotropic yield function (18) with associated flow rule and strain hardening. In an increment form, the macroscopic stress increments $\Delta\Sigma_{ij}$ are related to elastic increments of strains as

$$\Delta\Sigma_{ij} = E_{ijkl}(\Delta e_{kl} - \Delta e^p_{kl}), \tag{23}$$

where E_{ijkl} is the homogenized elasticity tensor. Using the associated flow rule, components of plastic strain increment are obtained as

$$\Delta e^p_{xx} = \Delta\lambda \frac{\partial \Phi}{\partial \Sigma_{xx}}, \qquad \Delta e^p_{yy} = \Delta\lambda \frac{\partial \Phi}{\partial \Sigma_{yy}}, \qquad \Delta e^p_{xy} = \Delta\lambda \frac{\partial \Phi}{\partial \Sigma_{xy}} \qquad \Delta e^p_{zz} = \Delta\lambda \frac{\partial \Phi}{\partial \Sigma_{zz}}. \tag{24}$$

Elimination of the flow parameter $\Delta\lambda$ from equations (24) results in the set of equations

$$\begin{gathered} \Delta e^p_{xx}\left(\frac{\partial \Phi}{\partial \Sigma_{yy}}\right) - \Delta e^p_{yy}\left(\frac{\partial \Phi}{\partial \Sigma_{xx}}\right) = 0, \qquad \Delta e^p_{xx}\left(\frac{\partial \Phi}{\partial \Sigma_{xy}}\right) - \Delta e^p_{xy}\left(\frac{\partial \Phi}{\partial \Sigma_{xx}}\right) = 0, \\ \Delta e^p_{xx}\left(\frac{\partial \Phi}{\partial \Sigma_{zz}}\right) - \Delta e^p_{zz}\left(\frac{\partial \Phi}{\partial \Sigma_{xx}}\right) = 0. \end{gathered} \tag{25}$$

With known increments of strain, the set of equation (25) together with the yield function equation (18) are solved iteratively by the Newton–Raphson method to obtain stress increments in the following steps.

(i) Initialize values of $\Delta\Sigma_{xx}$, $\Delta\Sigma_{yy}$, $\Delta\Sigma_{zz}$ and $\Delta\Sigma_{xy}$ by using $\Delta\Sigma_{ij} = E_{ijkl}\Delta e_{kl}$.

(ii) Calculate the gradient $(\partial\Phi/\partial\Sigma_{ij})$ of yield function and solve for the increments of plastic strain Δe^p_{xx}, Δe^p_{yy}, Δe^p_{zz} and Δe^p_{xy} from equations (25) and (18). Update the stresses, void volume fraction and plastic work using the relation.

$$\Delta W_p = \Sigma_{xx}\Delta e^p_{xx} + \Sigma_{yy}\Delta e^p_{yy} + \Sigma_{zz}\Delta e^p_{zz} + \Sigma_{xy}\Delta e^p_{xy}. \tag{26}$$

(iii) Update all parameters using the updated plastic work.

(iv) If $\Phi \leqslant \mathrm{tol}_1$ and correction to plastic strain increment is $\delta e^p_{ij} \leqslant \mathrm{tol}_2$, where tol_1, tol_2 are prescribed tolerances, then stop. Otherwise go to step (ii).

3.4. Numerical examples

The macroscopic anisotropic GTN model is validated by comparing the results of different macroscopic numerical simulations with those obtained by coupled macro–micro scale analysis using E-VCFEM and homogenization. Simulations are conducted for two different heterogeneous microstructural RVEs, without and with voids. The RVEs considered are (i) a square matrix domain with one circular particle as shown in figure 5(*a*) and (ii) an arbitrary shaped periodic domain with 17 randomly distributed elliptical particles of different sizes and shapes as shown in figure 5(*b*). The RVE material properties for the matrix are $E = 66\,\mathrm{GPa}$, $v = 0.33$. The post-yield behaviour for the pure matrix material without voids is expressed by the Ramberg–Osgood law ($\sigma_m = \sigma_0(\varepsilon^p_m/\alpha\varepsilon_0)^{1/n}$), where the initial flow stress is $\sigma_0 = 440\,\mathrm{MPa}$, ε_0 is the strain at yield ($\varepsilon_0 = \sigma_0/E$), material parameter $\alpha = 3/7$ and the strain hardening exponent $n = 12.5$. For the brittle particles, $E = 400\,\mathrm{GPa}$ and $v = 0.2$.

3.4.1. Simulations with the anisotropic plasticity model for microstructure without voids. Anisotropy parameters for the two RVEs are plotted in figures 6(*a*) and 7(*a*) as functions of W_p. Results of a pure macroscopic analysis using the anisotropic plasticity model of equations (18), (19), (23) and (24) are compared with pure micromechanics based results that are averaged after each load step. The results of this comparison for the loading condition ($e_{xx} : e_{yy} : e_{xy} = 4 : 1 : 4$) are compared in figures 6(*b*) and 7(*b*) with excellent agreement. Excellent agreement is also obtained for the loading conditions represented by various strain combinations that are not shown.

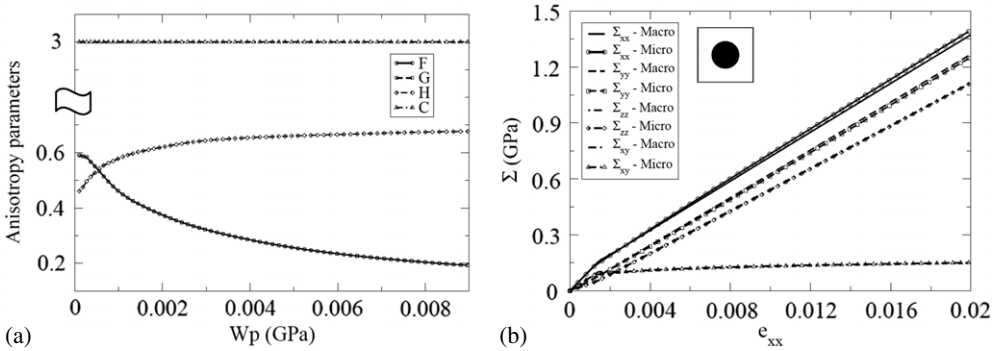

Figure 6. (*a*) Anisotropic plastic yield parameters, (*b*) comparison of stress–strain response by the macroscopic constitutive model with that by microscopic RVE analysis with homogenization for a simple unit cell model with one particle.

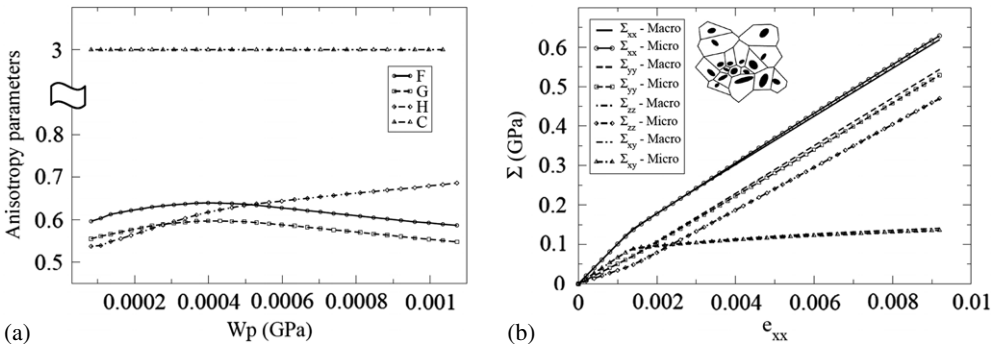

Figure 7. (*a*) Anisotropic plastic yield parameters, (*b*) comparison of stress–strain response by the macroscopic constitutive model with that by microscopic RVE analysis with homogenization for an arbitrary RVE with 17 random distributed elliptical particles.

3.4.2. Simulations with the anisotropic plasticity-damage model for microstructure with voids. The same simulations of section 3.4.1 are revisited for the two RVEs, now with 0.1% initial void volume fraction. The evolutions of parameters Q_1, Q_a, Q_b and Q_c with W_p are shown in figures 8(*a*) and 9(*a*). Results of simulations by the anisotropic ductile damage model are compared with those by micromechanical RVE analysis followed by homogenization, for the loading condition $e_{xx} : e_{yy} : e_{xy} = 4 : 1 : 4$ in figures 8(*b*) and 9(*b*). The results show good agreement. Additional calibrations and simulations are done for the RVE with two aligned long particles. Comparisons are shown in figure 10.

4. Conclusions

This paper develops two modules contributing to the overall framework of multi-scale modelling of ductile fracture of particle reinforced metallic materials, e.g. discretely reinforced aluminium. The first module is for detailed micromechanical analysis of particle fragmentation and matrix cracking of heterogeneous microstructures leading to ductile failure. This module is necessary for RVE level analysis with periodicity (level 1) as well as pure micromechanical analysis in regions where periodicity ceases to hold (level 2) in the multi-level analysis

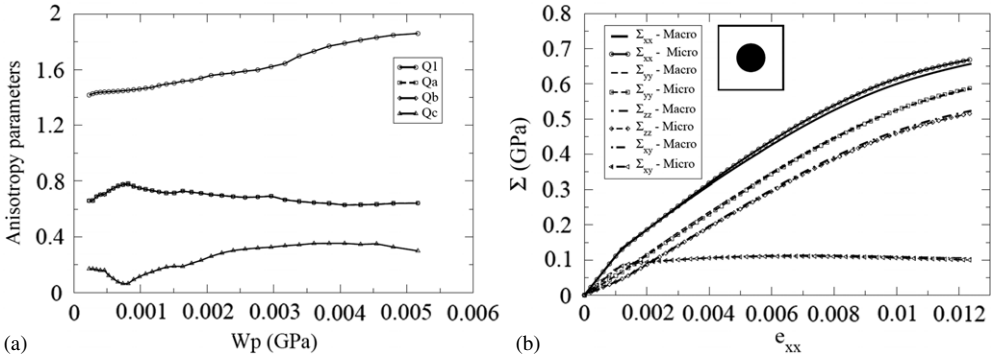

Figure 8. (*a*) Anisotropic parameters for the hydrostatic portion of plastic yield, (*b*) comparison of stress–strain response by the macroscopic constitutive model with that by microscopic RVE analysis with homogenization for a simple unit cell with one particle.

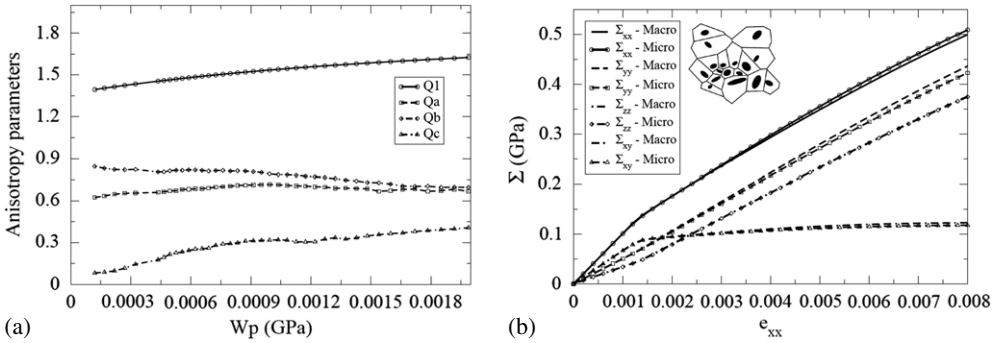

Figure 9. (*a*) Anisotropy parameters for the hydrostatic portion of plastic yield, (*b*) comparison of stress–strain response by the macroscopic constitutive model with that by microscopic RVE analysis with homogenization for an RVE with 17 random distributed elliptical particles.

discussed in [20, 23]. The Voronoi cell FEM for particle fragmentation is extended in this paper to incorporate ductile failure through matrix cracking in the form of void growth and coalescence using a non-local GTN model. In the resulting enriched VCFEM or E-VCFEM, the assumed stress-based hybrid VCFEM formulation is overlaid with narrow bands of displacement based elements to accommodate strain softening in the constitutive behaviour. Numerical examples presented show the potential of E-VCFEM in accurate microstructural modelling of ductile fracture.

The second module in this paper develops an anisotropic plasticity-damage model for macroscopic analysis in the multi-scale material model. The anisotropic model is taken to be in the form of the GTN model. Parameters in this model are calibrated from results of homogenization of microstructural variables obtained by E-VCFEM analysis of microstructural RVE containing particles, matrix and voids. Numerical examples are simulated with this model for different RVEs undergoing a wide variety of load paths. Comparison between the anisotropic GTN model and homogenized micromechanics results shows excellent agreement. Thus, the model is suitable for being implementing in macroscopic finite element codes to represent ductile failure in composites as long as the basic RVE assumptions remain valid. The authors are currently working on integrating these modules in a comprehensive multi-scale framework, which will be reported in subsequent papers [30].

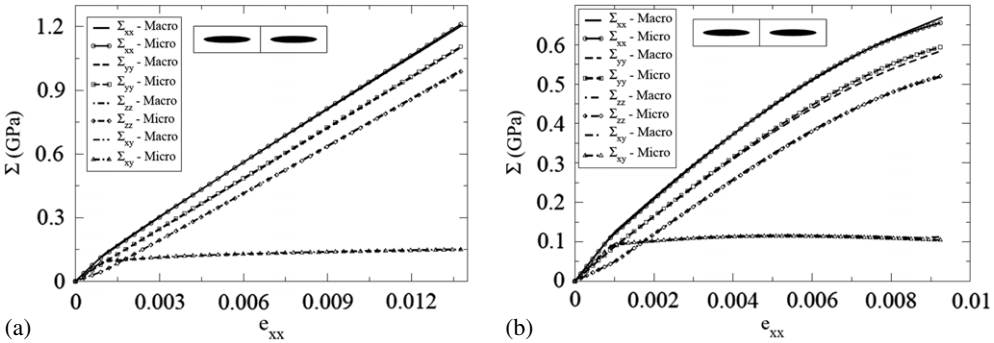

Figure 10. Comparison of strain–stress response by the macroscopic constitutive model with that by microscopic RVE analysis with homogenization for RVE with two aligned particles (*a*) without void, (*b*) with void.

Acknowledgments

This work has been supported by the National Science Foundation NSF Division of Civil and Mechanical Systems Division through the GOALI Grant No CMS-0308666 (Program director: Jorn Larsen-Basse). This sponsorship is gratefully acknowledged. Computer support by the Ohio Supercomputer Center through Grant PAS813-2 is also gratefully acknowledged.

References

[1] Ghosal A K and Narasimhan R 1996 Mixed-node fracture initiation in a ductile material with a dual population of second-phase particles *Mater. Sci. Eng.* A **211** 117–27
[2] Steglich D and Brocks W 1997 Micromechanical modeling of the behavior of ductile materials including particles *Comput. Mater. Sci.* **9** 7–17
[3] Llorca J and Gonzalez C 1998 Microstructural factors controlling the strength and ductility of particle reinforced metal–matrix composites *J. Mech. Phys. Solids* **46** 1–28
[4] Ghosh S and Moorthy S 1998 Particle fracture simulation in non-uniform microstructures of metal–matrix composites *Acta Mater.* **46** 965–82
[5] Moorthy S and Ghosh S 1998 A Voronoi cell finite element model for particle cracking in elastic–plastic composite materials *Comput. Methods Appl. Mech. Eng.* **151** 377–400
[6] Li S and Ghosh S 2004 Debonding in composite microstructures with morphological variations *Int. J. Comput. Methods* **1** 121–49
[7] Leblond J B, Perrin G and Devaux J 1994 Bifurcation effects in ductile metals with nonlocal damage *J. Appl. Mech.* 61 236–42
[8] Tvergaard V and Needleman A 1995 Effect of non-local damage in porous plastic solids *Int. J. Solids Struct.* **32** 1063–77
[9] Tvergaard V and Needleman A 1997 Nonlocal effects on localization in a void-sheet *Int. J. Solids Struct.* **34** 2221–38
[10] Rice J R 1976 The localization of plastic deformation *Proc. 14th Int. Congr. on Theoretical and Applied Mechanics (Delft) (Amsterdam: North-Holland/New York)* pp 207–20
[11] Chien W Y, Pan J and Tang S C 2001 Modified anisotropic Gurson yield criterion for porous ductile sheet metals *J. Eng. Mater. Technol.* **123** 409–16
[12] Benzerga A A, Besson J and Pineau A 2004 Anisotropic ductile fracture: II. Theory *Acta Mater.* **52** 4639–50
[13] Benzerga A A, Besson J 2001 Plastic potential for anisotropic porous solids *Eur. J. Mech.* A **20** 397–434
[14] Benzerga A A, Besson J, Batisse R and Pineau A 2002 Synergistic effects of plastic anisotropy and void coalescence on fracture mode in plane strain *Modelling Simul. Mater. Sci. Eng.* **10** 73–102
[15] Aravas N 1987 On the numerical integration of a class of pressure-dependent plasticity models *Int. J. Numer. Methods Eng.* **24** 1395–416

[16] Bass J M and Oden J T 1987 Adaptive finite element methods for a class of evolution problems in visco-plasticity *Int. J. Eng. Sci.* **6** 623–53
[17] Hughes T J R 1980 Generalization of selected integration procedures to anisotropic and nonlinear media *Int. J. Numer. Methods Eng.* **15** 1413–8
[18] Green A E and Naghdi P M 1965 A general theory of an elastic–plastic continuum *Arch. Ration Mech. Anal.* **18** 251–81
[19] Li M, Ghosh S and Richmond O 1999 A experimental-computational approach to the investigation of damage evolution in discontinuously reinforced aluminum matrix composite *Acta Mater.* **47** 3515–32
[20] Chu C C and Needleman A 1980 Void nucleation effects in biaxially stretched sheets *J. Eng. Mater. Technol.* **102** 249–56
[21] Tvergaard V 1981 Influence of voids on shear band instabilities under plane strain conditions *Int. J. Fract. Mech.* **17** 389–407
[22] Ghosh S and Kikuchi N 1991 An arbitrary Lagrangian–Eulerian finite element method for large deformation analysis of elastic–viscoplastic solids *Comput. Methods Appl. Mech. Eng.* **86** 127–88
[23] Zienkiewicz O C and Zhu J Z 1992 The superconvergent patch recovery and a posteriori error estimates: 1. The recovery technique *Int. J. Numer. Methods Eng.* **33** 1331–64
[24] Ghosh S, Lee K. and Raghavan P A multi-level computational model for multiscale damage analysis in composite and porous materials 2001 *Int. J. Solids Struct.* **38** 2335–85
[25] Swaminathan S, Ghosh S and Pagano NJ 2006 Statistically equivalent representative volume elements for composite microstructures: I. Without damage *J. Compos. Mater.* **40** 583–604
[26] Swaminathan S and Ghosh S 2006 Statistically equivalent representative volume elements for composite microstructures: II. With evolving damage *J. Compos. Mater.* **40** 605–21
[27] Raghavan P and Ghosh S 2004 Concurrent multi-scale analysis of elastic composites by a multi-level computational model *Comput. Methods Appl. Mech. Eng.* **193** 497–538
[28] Hill R A 1948 A theory of yielding and plastic flow of anisotropic metals *Proc. R. Soc. Lond. Ser. A* **193** 281–97
[29] Chao H and Ghosh S 2007 Enriched Voronoi cell FEM for ductile fracture in particle reinforced metallic materials submitted
[30] Bai J and Ghosh S 2007 Homogenization based anisotropic continuum damage mechanics model for ductile failure in metallic materials with voids submitted